Article

Mixing of miscible shear-thinning fluids in a lid-driven cavity

Junhao Wang [1, 2], Shugang Ma [3], Peng Chen [1, 2], Zhipeng Li [1, 2, *], Zhengming Gao [1, 2, *], J.J. Derksen [4]

[1] Beijing Advanced Innovation Center for Soft Matter Science and Engineering, Beijing University of Chemical Technology, Beijing 100029, China

[2] State Key Laboratory of Chemical Resource Engineering, School of Chemical Engineering, Beijing University of Chemical Technology, Beijing 100029, China

[3] PetroChina Petrochemical Research Institute, Beijing 102206, China

[4] School of Engineering, University of Aberdeen, Aberdeen AB24 3UE, UK

* Corresponding author. Tel.: +8610 64418267; fax: +8610 64449862. E-mail address: lizp@mail.buct.edu.cn (Z. Li), gaozm@mail.buct.edu.cn (Z. Gao)

Abstract

The concentration and velocity fields of two refractive index matched miscible shear-thinning fluids in a lid-driven cavity were investigated by using planar laser-induced fluorescence and particle image velocimetry, as well by computational fluid dynamics. Quantitative analyses show that the results obtained by flow simulations with the species transport model are in good agreement with the experimental results. The effects of different parameters were studied by using the intensity of segregation. For two fluids with the same rheological parameters, the relative amounts of liquids H_1/H and the power-law index n dominate the mixing process while the Reynolds number Re plays a marginal role. As for two fluids with density difference, buoyancy has significant influence on the mixing process. The dimensionless group $\frac{Ar}{Re}$ (redefined such as to include shear thinning behavior) is proposed for assessing the effect of buoyancy and rheological properties on the mixing of miscible shear-thinning fluids.

Highlights

· Dimensional analyses on the mixing of miscible shear-thinning fluids were elaborated.

· Mixing of two refractive index matched shear-thinning fluids were measured using PLIF.

· Simulated velocity and concentration fields agree well with experimental results.

· The group *Ar*/*Re* for shear-thinning fluids was proposed to quantify buoyancy effect.

Keywords: Shear-thinning fluid; Mixing of miscible fluids; Particle image velocimetry; Planar laser-induced fluorescence; Species transport model; Lid-driven cavity

Nomenclature

C_1	mass fraction of Liquid 1
D	diffusion coefficient, $m^2 \cdot s^{-1}$
F	fluorescence intensity, cd
g	gravitational acceleration vector, $m \cdot s^{-2}$
H	height of the cavity, m
H_1	height of Liquid 1, m
I	excitation intensity, cd
I_{sat}	saturation intensity, cd
k	consistency index, $Pa \cdot s^n$
L	length of the cavity, m
n	power-law index,
P	pressure, Pa
t	time, s
U	lid speed, $m \cdot s^{-1}$
Ut/L	dimensionless time,
$\boldsymbol{u}$	velocity vector, $m \cdot s^{-1}$
u	velocity in x direction, $m \cdot s^{-1}$
v	velocity in y direction, $m \cdot s^{-1}$
w	velocity in z direction, $m \cdot s^{-1}$
W	width of the cavity, m
x,y,z	Cartesian coordinates, m
$\boldsymbol{\gamma}$	shear rate, s^{-1}
$\boldsymbol{\gamma}_c$	characteristic shear rate, $\frac{U}{L}$, s^{-1}
δ	scalar diffusion distance, m
Δ	shear rate tensor, s^{-1}

μ	apparent viscosity, $k\boldsymbol{\gamma}^{n-1}$, Pa·s
μ_c	characteristic apparent viscosity, $k\boldsymbol{\gamma}_c{}^{n-1}$, Pa·s
ρ	density, kg·m^{-3}
$\Delta\rho$	density difference, $\rho_1 - \rho_2$, kg·m^{-3}
$\boldsymbol{\tau}$	stress tensor, Pa

1. Introduction

Mixing of non-Newtonian fluids is very common in chemical engineering applications, such as polymer blending and fabric dyeing [1]. Many materials involved in polymer industry are highly viscous non-Newtonian fluids and the mixing process is often carried out in special mixers such as cavity transfer mixers or twin-screw extruders [2,3]. Due to the complex geometries of these mixers, it is difficult to visualize the mixing process directly. Therefore, the structures of these mixers are often simplified as lid-driven cavity (LDC) or Taylor-Couette cell for fundamental experimental and simulation studies [4–7].

Lid-driven cavity has simple structure and it is often used for verification of simulation methods [8–11]. A cavity filled with a single non-Newtonian fluid has been studied extensively for wide ranges of power-law parameters *k* and *n* [12–15]. In recent years, simulation research on non-Newtonian fluids in LDCs focused on heat transfer as well as mixing behavior. Selimefendigil and Chamkha studied the heat transfer capacity of non-Newtonian fluids with power-law index *n* ranging from 0.6 to 1.4 under natural convection and magnetic forces at different angles [16]. Kefayati studied the concentration, temperature, and streamline distributions with *n* varying from 0.2 to 1 [17,18]. The results show that heat and mass transfer capabilities increase with increasing power-law index.

Several visualization experiments in LDCs have been reported. Mills added detergent to oil and measured the streamlines in cavities with different aspect ratios [19]. Koseff and Street used the thymol blue technique and laser-Doppler-anemometry (LDA) to visualize the flow field [20,21]. With the development of visualization techniques, planar laser-induced fluorescence (PLIF) and particle image velocimetry (PIV) have become reliable techniques to measure concentration and velocity fields, respectively. Liberzon *et al*. measured the steady state and unsteady state flow in LDCs by using the PIV technique [22,23]. Hoefsloot *et al*. added different amounts of polyacrylamide to glycerol to configure two types of shear-thinning fluids and measured the concentration field in LDCs by using the PLIF technique [24]. The results suggest that

mixing is enhanced if the motion of the lid is applied to the more viscous liquid.

As most of the research focused on the flow characteristics of single fluid, quantitative studies on the mixing behavior of two miscible shear-thinning fluids in an LDC have not been rigorously investigated yet. In addition, the effect of density difference on the mixing process of miscible shear-thinning fluids has not been reported.

The work of this paper is a continuation of our previous work on the mixing of two miscible Newtonian fluids with different densities [25]. Previous work has shown that a dimensionless number $\frac{Ar}{Re}$ characterizes the mixing process of two Newtonian fluids with density difference. $\frac{Ar}{Re}$ is defined as the ratio of buoyancy ($\Delta\rho gL^3$) to viscous force (μUL), with μ the viscosity of Newtonian fluids. The mixing processes having the same $\frac{Ar}{Re}$ are essentially the same and the larger $\frac{Ar}{Re}$, the worse the mixing performance. The primary aim of this paper is to study the mixing behavior of two miscible shear-thinning fluids with density difference in an LDC by using PLIF and PIV. The second aim is to validate our simulation approach with the experimental results. Thirdly, based on dimensional analyses and the validated simulation methods, we will investigate the effects of different operating and physical parameters on the mixing process in detail.

This paper is organized as follows: in the next section, based on dimensional analyses on the mixing in a lid-driven cavity, the parameter space in terms of dimensionless number are analyzed systematically. We then present the PLIF and PIV experimental setups. After that, we introduce the numerical methods and discuss the numerical strategy. In the section of the results and discussion, concentration and velocity fields of two shear-thinning fluids measured using the PLIF and PIV techniques are analyzed and utilized to validate the simulated results. The differences between Newtonian fluids and shear-thinning fluids are identified next. The effects of different operating and physical parameters are also analyzed. The final section summarizes the conclusions and discusses future research.

2. Dimensional Analyses

A square lid-driven cavity with side-length L, lid speed U, and Newtonian liquid with density ρ and viscosity μ is fully characterized by one Reynolds number $Re = \frac{\rho UL}{\mu}$. Adding a second liquid with the same viscosity but a different density gives rise to a second dimensionless number $\frac{Ar}{Re} = \frac{\Delta\rho gL^3}{\mu^2/\rho_1}\frac{\mu}{\rho_1 UL} = \frac{\Delta\rho gL^2}{\mu U}$ with $\Delta\rho = \rho_1 - \rho_2$ the density difference between two liquids and $Ar = \frac{\Delta\rho gL^3}{\mu^2/\rho_1}$ the Archimedes number. Adding

a second liquid also means that the flow system also depends on the relative amount of liquids and the way they are initially placed in the cavity. Note that the relative amount is another dimensionless number. Giving the two liquids – in addition to a different density – also a different viscosity now leads to yet another dimensionless number – the viscosity ratio $\eta = \frac{\mu_1}{\mu_2}$. For two Newtonian liquids we thus now have a parameter space of three dimensionless numbers plus the initial placement and relative amounts of liquids.

Now we move to power-law liquids for which $\mu = k\boldsymbol{\gamma}^{n-1}$, where μ is apparent viscosity, $\boldsymbol{\gamma}$ is shear rate, *k* is consistency index, and *n* is the power-law index which is dimensionless. With a single liquid the cavity flow is now fully characterized by two dimensionless numbers. The Reynolds number is obtained as $Re = \frac{\rho UL}{k\boldsymbol{\gamma}_c{}^{n-1}} = \frac{\rho U^{2-n}L^n}{k}$ by first defining a characteristic shear rate $\boldsymbol{\gamma}_c = \frac{U}{L}$ and then defining a characteristic apparent viscosity $\mu_c = k\boldsymbol{\gamma}_c{}^{n-1}$. Next to *Re*, the second dimensionless number is *n*. With two power-law liquids that only differ in terms of their densities, we need to add another dimensionless number which could be $\frac{Ar}{Re} = \frac{\Delta\rho g L^2}{Uk_1\boldsymbol{\gamma}_c{}^{n_1}} = \frac{\Delta\rho g L^{n+1}}{kU^n}$. This is based on the notion of characteristic shear rate $\boldsymbol{\gamma}_c = \frac{U}{L}$ and characteristic apparent viscosity $\mu_c = k\boldsymbol{\gamma}_c{}^{n-1}$. As before for Newtonian liquids, adding a second liquid also means that the flow system now also depends on the relative amount of liquids and the way they are initially placed in the cavity. Two different power-law liquids that – in addition to different density – also have different *k* and *n* will add two additional dimensionless numbers making a total of five: $Re = \frac{\rho U^{2-n}L^n}{k}$, $\frac{Ar}{Re} = \frac{\Delta\rho g L^{n+1}}{kU^n}$, n_1, n_2, $\frac{k_1}{k_2}$.

As an essential variable that affects the mixing performance of miscible fluids, yet another dimensionless Schmidt number $Sc = \frac{k_1\boldsymbol{\gamma}_c{}^{n_1-1}}{\rho_1 D}$ is considered. The smallest Schmidt number is 6.1×10^5 in this study. Besides, Peclet number $Pe = ScRe = \frac{UL}{D}$, which determines whether mass transfer is controlled by convection or diffusion, is much larger than 1 in all cases. As a result, Schmidt numbers and Peclet numbers are much greater than 1 and the effects of mass diffusion on mixing efficiency could be ignored [26].

3. Experiment

3.1. Flow system

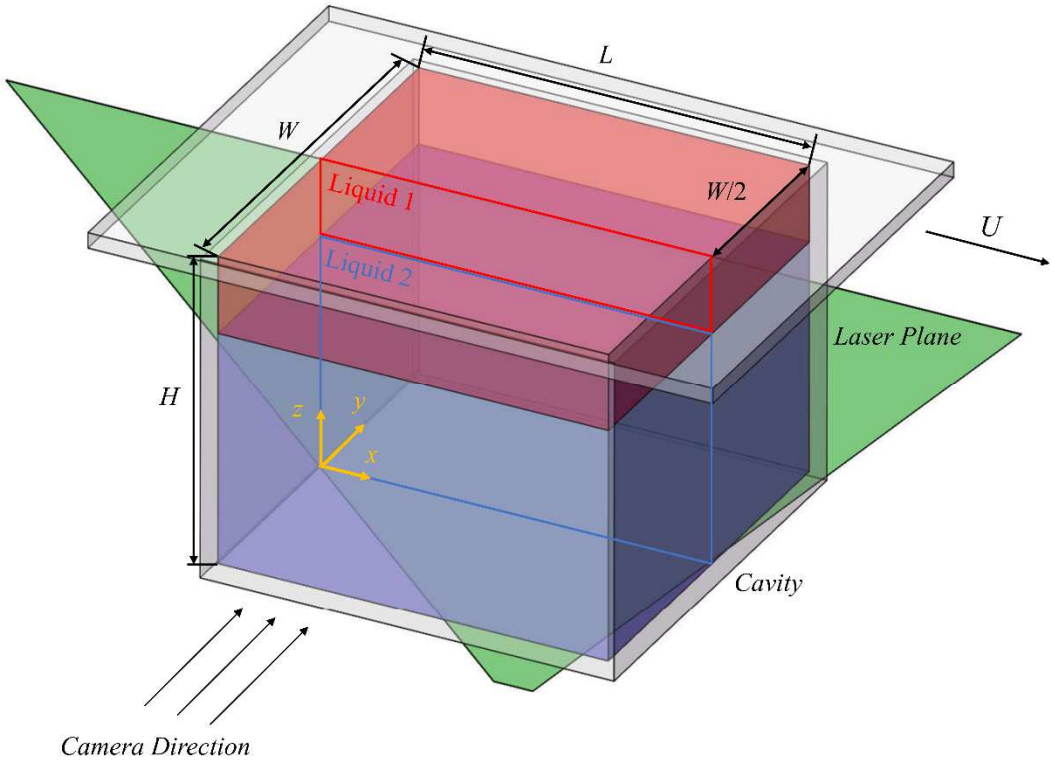

Fig. 1. Schematic diagram of the experimental setup and the Cartesian coordinate system.

As shown in Fig. 1, a transparent lid-driven cavity with $L = W = 1.25H = 0.05$ m made of polymethyl methacrylate (PMMA) was filled with two miscible shear-thinning liquids. A self-encoding stepping motor (Shanghai Zhengji, China) was used to move the lid at specified speed, and the fluctuations of the speed are less than 1% in the experiments. The Cartesian coordinate system is shown in Fig. 1, and the velocities in the x, y, z directions are represented by u, v, and w, respectively. The lid moved along the x-direction and its speed U is 0.02 m·s^{-1}. The maximum displacement of the lid is 0.35 m. As shown in Fig. 1, the measurement plane of the experiment is the y=0 plane.

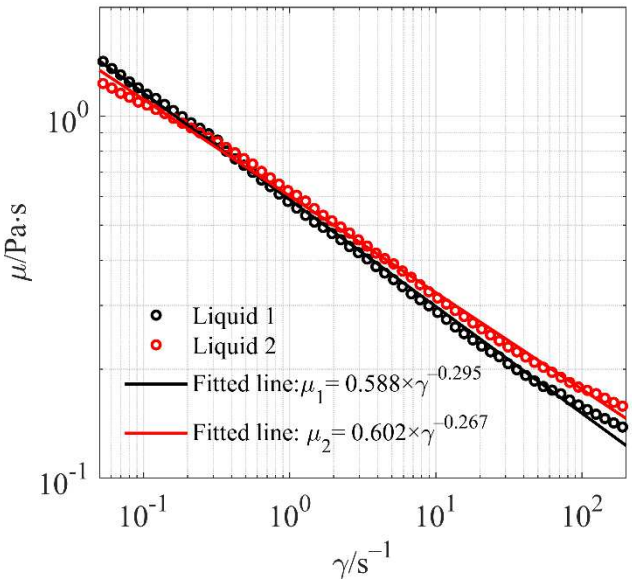

Fig. 2. Viscosities of two miscible shear-thinning fluids as a function of shear rate at 21 □.

Table 1 Properties of two shear-thinning fluids at 21□

	PAAS(0.1%) - sucrose - water solution	Density /kg·m^{-3}	k /Pa·s^n	n	Refractive index	Liquid height
Liquid 1	61.5% (mass) sucrose	1296	0.588	0.705	1.45	0.25H
Liquid 2	63.0% (mass) sucrose	1306	0.602	0.733	1.45	0.75H

The working fluids were made of sodium polyacrylate (PAAS) (Shanghai Macklin, China), deionized water, and sucrose (Sinopharm Chemical Reagent Co., China). The mass fractions of sucrose for Liquid 1 and Liquid 2 are 61.5% and 63%, respectively. The rheological properties of the fluids were measured by using a MARS40 Rheometer (Haake, Germany). Fig. 2 shows the apparent viscosities of the working fluids as a function of shear rates ranging from 0.05 to 200 s^{-1} at 21□, which is the temperature of the visualization experiments. Power-law model $\mu = k\boldsymbol{\gamma}^{n-1}$ could be utilized to represent the apparent viscosities, and the results are shown in Table 1. The coefficients of determination R^2 of the two fitted linear relationships are both larger than 0.998.

The refractive indices of the two liquids need to be matched to avoid optical distortion in the experimental measurements. The refractive indices were measured by using the Abbe refractometer (Shanghai INESA Instrument, China). The refractive index difference between the two working liquids is about 0.1% at 21□, which means the indices are well matched.

3.2. Visualization experiment and image processing

The PIV measurement system (Dantec, Denmark) consists of a laser (Dual Power, 100 mJ, 100 Hz, 532 nm), a CMOS camera (Speed Sensing 4 MP, 193 Hz, 2320×1720 pixels), a synchronizer, and dynamic studio software. Hollow glass beads (TSI, USA) were used as the PIV tracers, with diameters of 8–12 μm and density of about 1500 $kg \cdot m^{-3}$. Rhodamine B was chosen as the PLIF tracer in Liquid 1, and its concentration was 50 $\mu g \cdot L^{-1}$.

In PIV experiments, the time interval between the two laser pulses multiplied by the lid speed should be less than one-quarter of the interrogation window size and of the laser thickness, and then the time interval was chosen as 7 ms. An adaptive interrogation window method was used to calculate the fluid velocity in the measurement plane. The size of the interrogation window is based on the compromise between robustness/precision and resolution [27]. The minimum size of the interrogation window is 48 pixel× 48 pixel, and the overlap rate is 50% in our PIV experiments. The image resolution is 30.27 μm per pixel, so the resolution of the velocity vectors is about 0.73 mm.

When the PLIF technique was used to measure the concentration field, the exposure time of the CMOS camera was set as 7 ms and the shooting frequency was 70 Hz. The time interval of two laser pulses is 14 ms. The absorption wavelength and maximum emission wavelength of Rhodamine B are about 532 nm and 590 nm, respectively [28]. Therefore, a sharp cut-off filter that blocks out the light with wavelength less than 550 nm was added in front of the camera to capture excited fluorescence only.

The PLIF technique quantifies the concentration field by using the relationship between the concentration of liquid and the fluorescence intensity [29].

$$F \propto \frac{I}{1+I/I_{sat}} C \tag{1}$$

where F is the fluorescence intensity, I is the excitation intensity, I_{sat} is the saturation intensity for the dye, and C is the local concentration. Since $I \ll I_{sat}$ in the experiment, Eq. (1) can be transformed to

$$F \propto IC \tag{2}$$

Fig. 3(a) shows the fluorescence intensity as a function of the concentration of Rhodamine B ranging from 0 to 60 $\mu g \cdot L^{-1}$ in our calibration experiments, and good linear relationship was obtained. Then, the fluorescence intensity measured by the CMOS camera could be converted to the concentration of the liquid with Rhodamine B (Liquid 1). Fig. 3(b) shows a gray-level image at initial stage of the experiments and its conversion to a pseudo-color image with concentration values. The blue color indicates that the mass fraction of Liquid 1 is 0, and the red color means that the mass fraction of Liquid 1 is 1. The horizontal and

the vertical coordinate are normalized by cavity length and cavity height, respectively. The mixing time is converted into a dimensionless time Ut/L.

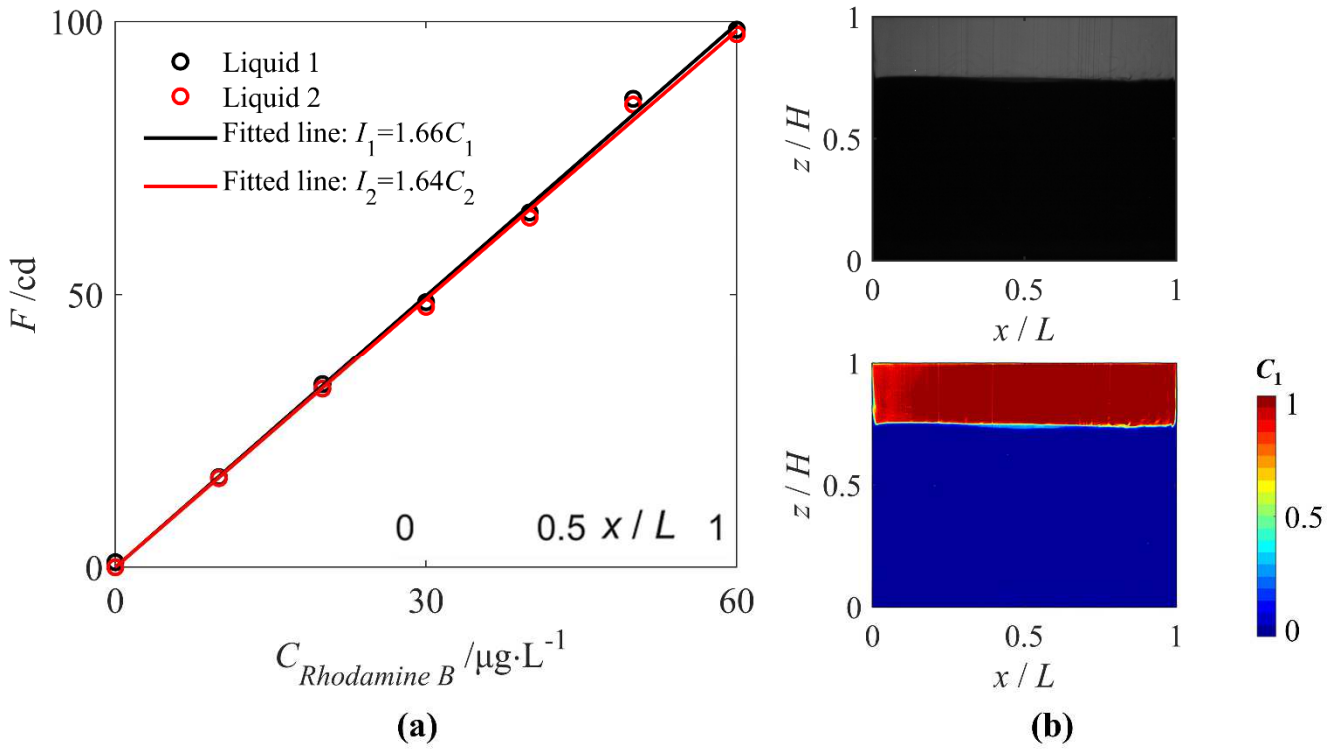

Fig. 3. (a) Fluorescence intensity induced by the laser in two shear-thinning fluids as a function of the concentration of Rhodamine B at 21 □, (b) initial distribution of the two fluids in the LDC with grayscale image and pseudo color image.

4. Simulation

As a generalized Newtonian fluid, shear-thinning fluids can be described by the continuity equation and the Cauchy's equation of motion:

$$\frac{\partial \rho}{\partial t} + \nabla \cdot (\rho \boldsymbol{u}) = 0 \tag{3}$$

$$\frac{\partial \rho \boldsymbol{u}}{\partial t} + \nabla \cdot (\rho \boldsymbol{u}\boldsymbol{u}) = -\nabla p + \nabla \cdot \tau + \rho \boldsymbol{g} \tag{4}$$

where p is the pressure, $\boldsymbol{u}$ is the velocity, $\boldsymbol{g}$ is the acceleration of gravity, and $\boldsymbol{\tau}$ is the stress tensor. The stress tensor in case of the power-law viscosity model is given by [30]:

$$\boldsymbol{\tau} = k|\Delta : \Delta|^{\frac{n-1}{2}}\Delta \tag{5}$$

where

$$\Delta = \frac{\nabla \boldsymbol{u} + \nabla \boldsymbol{u}^{\boldsymbol{T}}}{2} \tag{6}$$

The shear rate $\boldsymbol{\gamma}$ is given by [31]:

$$\boldsymbol{\gamma} = \sqrt{\mathbf{2}\Delta : \Delta} \tag{7}$$

A species transport model was used to simulate the mixing process of two miscible shear-thinning fluids in the LDC. The conservation equation of species 1 is [32]:

$$\frac{\partial}{\partial t}(\rho C_1) + \nabla \cdot (\rho \boldsymbol{u} C_1) = \nabla \cdot (\rho D \nabla C_1) \tag{8}$$

where C_1 is the mass fraction of species 1, D is the diffusion coefficient and is set as 1×10^{-10} $m^2 \cdot s^{-1}$ according to Adamson's experimental results for sucrose-water solution [33]. The mass fraction of species 2 is:

$$C_2 = 1 - C_1 \tag{9}$$

The density of the mixture follows the volume-weight-mixture-law:

$$\frac{1}{\rho} = \frac{C_1}{\rho_1} + \frac{1 - C_1}{\rho_2} \tag{10}$$

The effective viscosity of the mixture is calculated by using the mass-weighted-mixing-law:

$$\mu = \mu_1 C_1 + \mu_2 (1 - C_1) \tag{11}$$

For the reason of numerical stability in our simulations, we limited the maximum apparent viscosity of Liquid 1 and Liquid 2 to 1.68 Pa·s and 1.60 Pa·s, respectively, when the shear rate is less than 0.02 s^{-1}. The simulated results show that the maximum shear rate in the cavity does not exceed 150 s^{-1}, which indicates the linear fittings shown in Fig. 2 are valid.

Cartesian coordinate and cavity geometries used in the simulations are the same as those in the experimental setup. Uniform hexahedral grid with 3.2 million cells and 3.15×10^{-4} m cell spacing was used in this study. In order to verify grid sensitivity, grids with 1.6 million cells and 6.4 million cells were also used and discussed in the next section.

The transient pressure-based solver was used based on the Ansys Fluent software. The gravitational acceleration was 9.81 m/s^2 in negative z direction. The third-order MUSCL (monotone upstream-centered schemes for conservation laws) scheme was used for the spatial discretization of species transport equations [34]. Spatial discretization of the momentum equation was based on the second-order upwind scheme, and the second-order implicit scheme was used for time advancement. The SIMPLE (semi-implicit method of

pressure link equation) algorithm was used to couple pressure and velocity [8,25]. The time step was ranged from 0.002 s to 0.005 s to keep the Courant-Friedrichs-Levy number smaller than 1 [35]. Convergence per time step was achieved when normalized residuals of the continuity, mass fraction, and velocities were less than 10^{-4}. The no-slip condition was applied at all walls.

5. Results and Discussion

5.1. Validating simulated velocity and concentration by using PIV and PLIF data

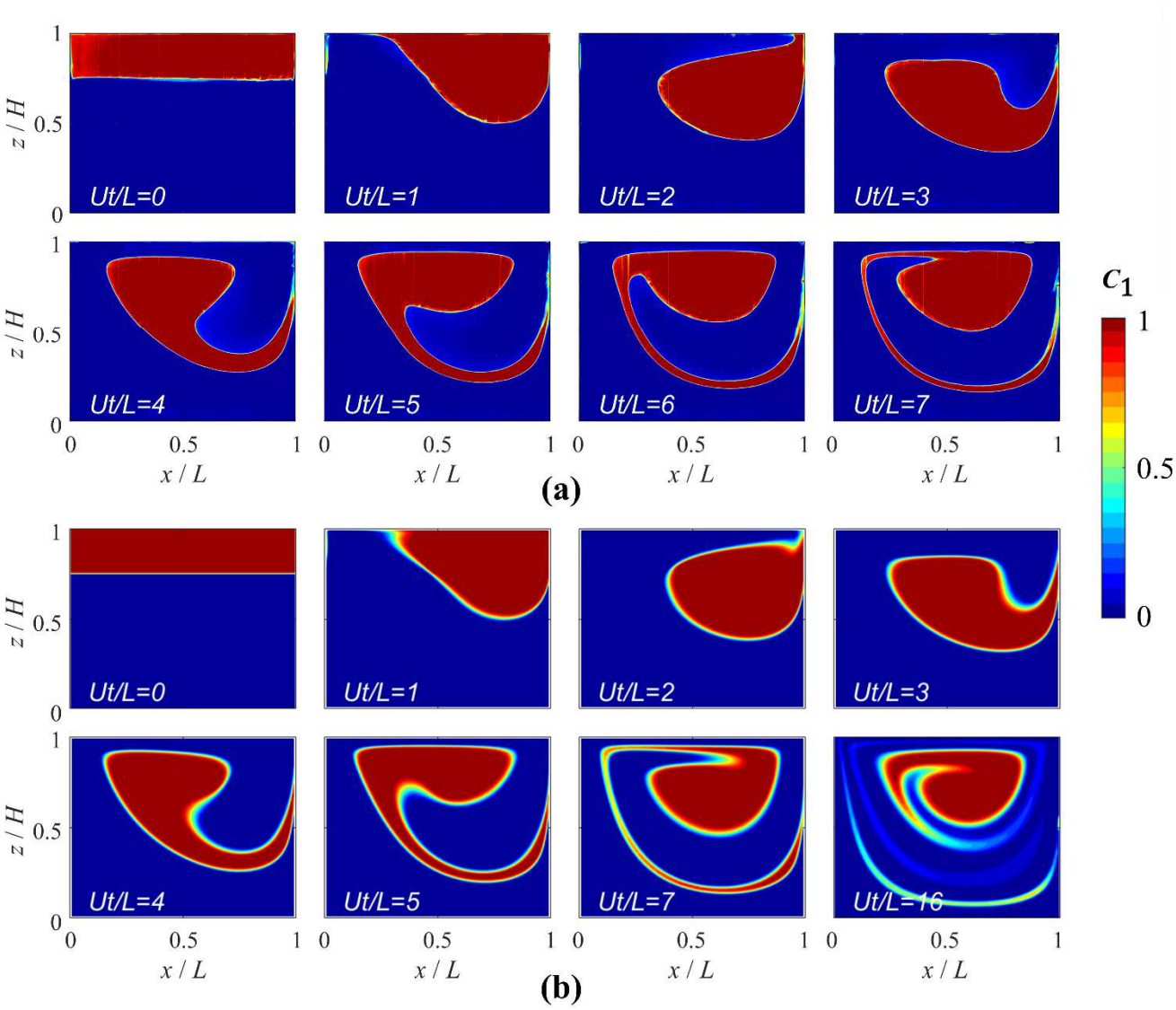

Fig. 4. Instantaneous concentration of Liquid 1 measured in the PLIF experiments (a) and predicted in the CFD simulations (b).

Fig. 4 shows the PLIF experimental and computational fluid dynamics (CFD) simulated instantaneous concentration of Liquid 1 in the plane $y/W = 0$ at different moments. We see that the time evolution of the mixing process of two miscible shear-thinning fluids in the simulation closely matches that in the experiment. At initial stage $Ut/L = 0$, the two shear-thinning fluids have a clear interface with Liquid 1 occupying 1/4 on the up layer and Liquid 2 filling the lower space of the cavity. As the lid moves, the fluid near the lid gets momentum from the moving lid and moves in positive x-direction. When the fluid encounters the wall on the right, the movement direction changes so that the upper-layer fluid that carries momentum moves downward. From $Ut/L = 3$ to $Ut/L = 7$, the lid drives more Liquid 2 to split Liquid 1 into one approximately semi-circular main body and one striation. In our simulation, we extended the mixing process to the moment $Ut/L = 16$, as shown in Fig. 4(b). It is found that the original region with Liquid 1 is further split by Liquid 2, and the Liquid 1 striation is continuously stretched and driven away from the main region, achieving mixing with Liquid 2.

Fig. 5 shows the velocity fields obtained in the PIV experiments and CFD simulations in the plane $y/W = 0$ at four moments. In order to demonstrate the interaction between velocity fields and concentration fields in the LDC, the concentration interface between Liquid 1 and Liquid 2 is also shown in Fig. 5, which is represented by the iso-lines with the Liquid 1 volume fraction of 0.9. At $Ut/L = 1$, the region with Liquid 1 is forced by the lid to move right and downward, and then Liquid 2 fills the top left region previously occupied by Liquid 1. At this moment, a nearly symmetrical velocity contour is forming along $x=L/2$, but the region with velocity larger than $0.2U$ is small. With the movement of the lid and increasing Ut/L, asymmetrical velocity contour is developed, and the region with velocity larger than $0.3U$ mainly appears in the top right of the cavity. Although the two liquids have different density and viscosity, there is no noticeable interface between the two liquids during the mixing process in the PIV experiments, as well as in CFD simulations.

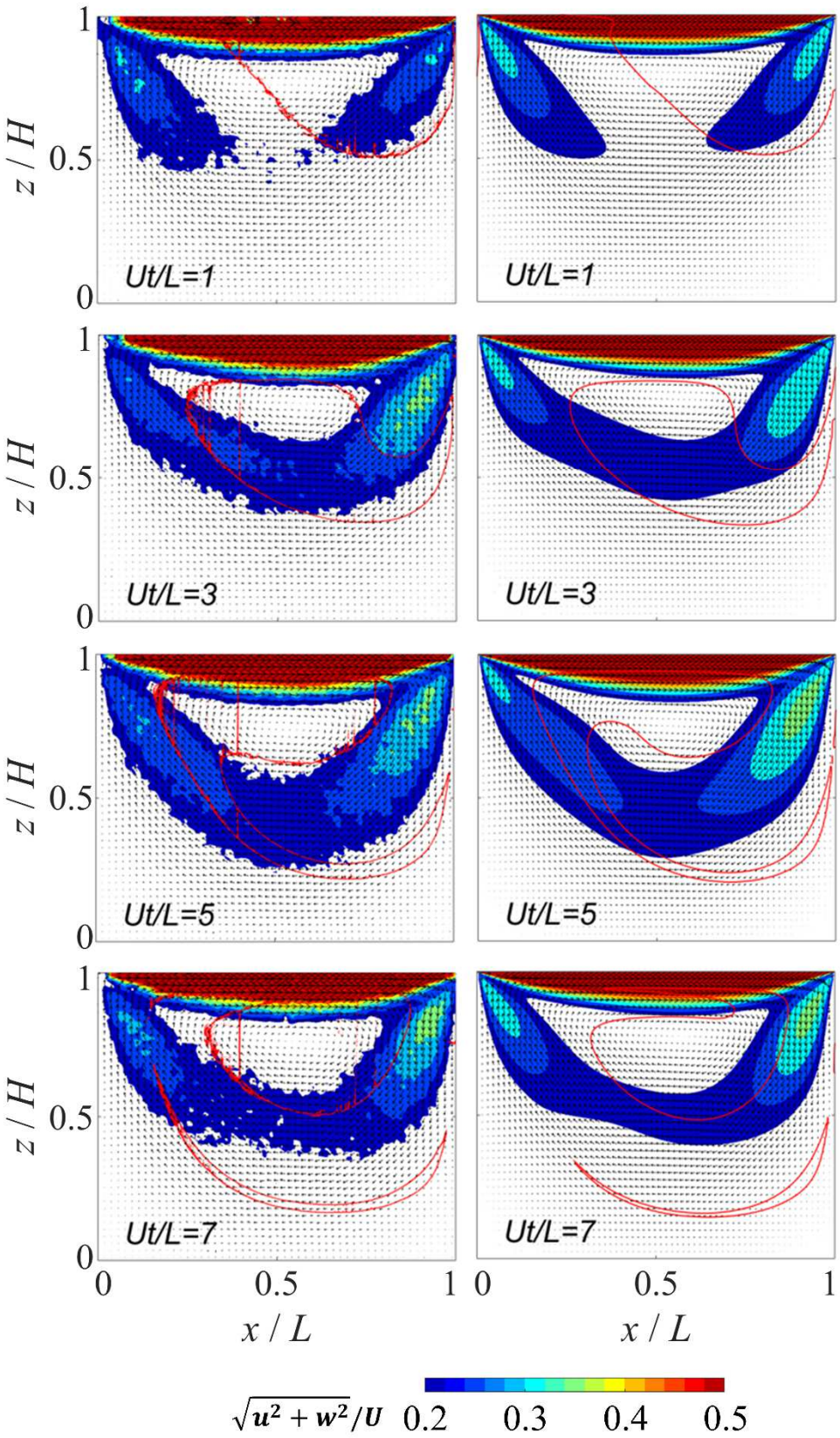

Fig. 5. Experimental (left column) and simulated (right column) instantaneous velocity field in the cavity with two miscible shear-thinning liquids. The distribution of Liquid 1 with volume fraction of 90% is marked by red lines in each panel. (ρ_1 = 1296 kg·m^{-3}, ρ_2 = 1306 kg·m^{-3}, $\mu_1 = 0.5876\dot{\gamma}^{-0.295}$ Pa·s, μ_2

$=0.6018\dot{\gamma}^{-0.267}$ Pa·s, $U = 0.02$ m·s^{-1}).

Simulated velocity profiles on lines $z/H = 0.75$ and $x/L = 0.5$ with different grids at $Ut/L = 7$ are shown in Fig. 6(a) and compared with PIV data. The three simulated velocity profiles overlap at $x/L = 0.5$ and agree well with the experimental profile. As for the simulated velocity profiles at $z/H = 0.75$, increasing grid from 1.6 million cells to 3.2 million cells gives better simulated data, which more approach the experimental results. Further increasing the grid to 6.4 million cells does not show improvements, that is, grid-independent velocity field could be obtained for grid with 3.2 million cells.

Fig. 6(b) shows the simulated concentration distributions on lines $z/H = 0.75$ and $x/L = 0.5$ with different grids at $Ut/L = 7$. The results show that the concentration field is much more sensitive to the cell spacing than the velocity field. The smaller the cell spacing, the more accurate the simulated concentration field. As mentioned above, the smallest Schmidt number could reach 6.1×10^{5} in this study. The scalar diffusion distance δ over the time for one lid passage L/U is $\delta/L = (ScRe)^{-0.5} = 3.16\times10^{-4}$. As a result, to capture the concentration in full detail, the number of cells should be of the order of $(L/\delta)^3 \approx 10^{10}$, which is beyond current computer hardware. In Fig. 6(b), simulated concentration profiles with 3.2 million cells are in good agreement with the experimental results, although there are some discrepancies near the lid at $x/L = 0.5$. As a compromise between accuracy and affordable computational resource, the rest of the simulations in this work are based on 3.2 million cells with cell spacing of 3.15×10^{-4} m.

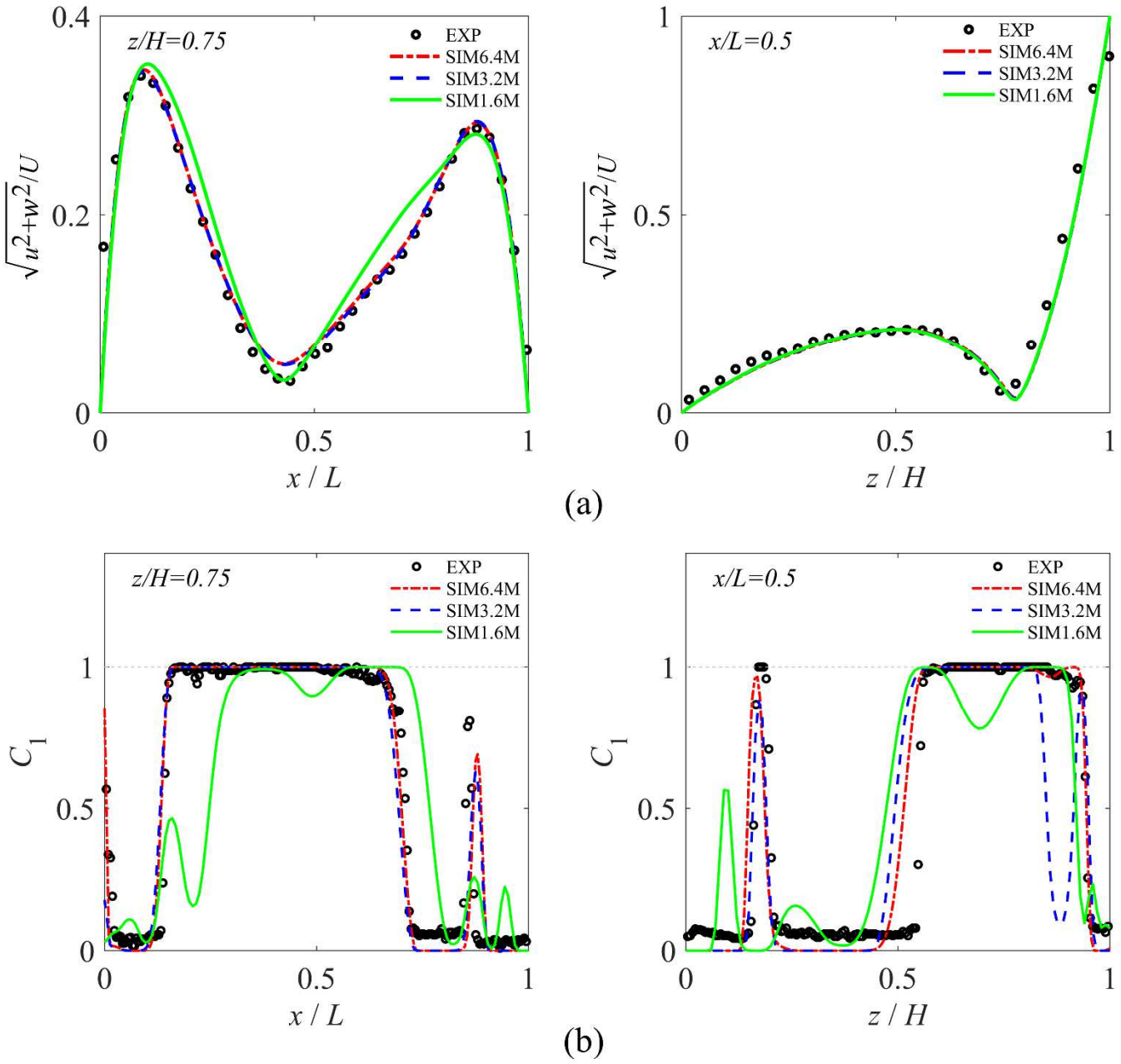

Fig. 6. Instantaneous velocity (a) and concentration (b) profiles with U = 0.02 m·s^{-1} at Ut/L=7. Simulated results with 1.6, 3.2, and 6.4 million cells are presented.

In summary, grid independent flow fields are achieved in our simulations by verifying with the PIV experimental data. Our simulations with the species transport model could predict the mixing process of two miscible shear-thinning fluids, and the simulated concentration distributions are in good agreement with the experimental data, despite grid converged concentration field has not yet been reached at this level of resolution. In the following sections, the validated simulation method will be used to discuss the mixing behavior of two miscible shear-thinning fluids.

5.2. Comparison between mixing behavior of shear-thinning fluid and Newtonian fluid

Compared with the simulated results of mixing two miscible Newtonian fluids in the LDC, the velocity fields and concentration fields of mixing two miscible shear-thinning fluid are different at constant *Re*. Fig. 7(a) shows the concentration fields of Liquid 1 in the plane $y/W = 0$ with the shear-thinning fluid and Newtonian fluid at $Ut/L = 7$ and $Re = 1.70$. After the lid moves for the same amount of time, the mixing process of Newtonian fluid develops faster and the striation of Liquid 1 is thinner, indicating that the mixing is more efficient. In Fig. 7(b), the region with velocity $\sqrt{u^2+w^2}/U > 0.2$ of the shear-thinning fluids is smaller than that of the Newtonian fluid. Moreover, the maximum velocity of Newtonian fluid in the upper left and right are larger than that of the shear-thinning fluid, which means the Newtonian fluids transfer momentum farther than the shear-thinning fluids.

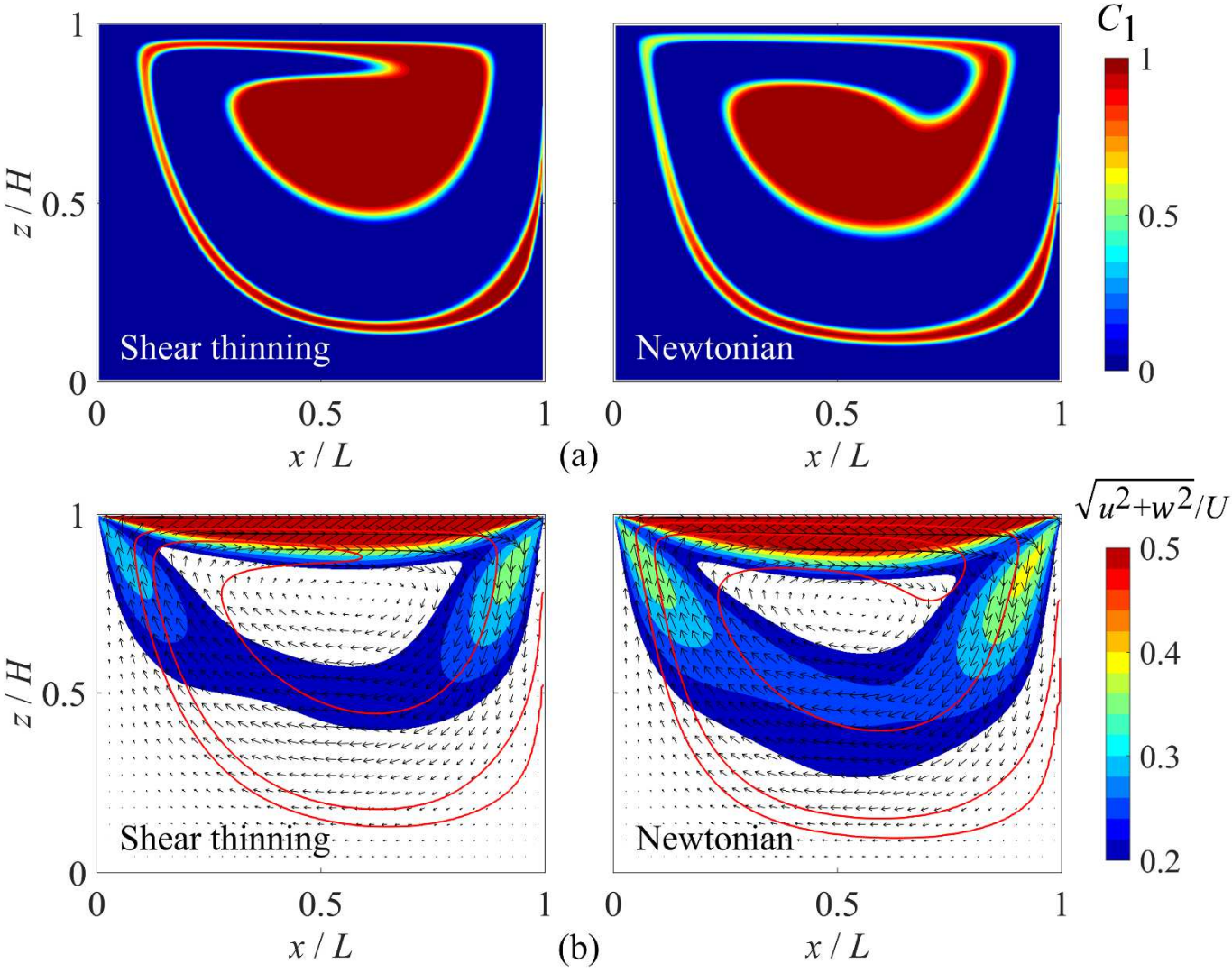

Fig. 7 Simulated instantaneous concentration (a) and velocity (b) fields of two miscible shear-thinning fluids and Newtonian fluids at Ut/L = 7 with constant Reynolds number Re=1.70. The distribution of Liquid 1 with volume fraction of 90% is marked by red lines in panel (b). The properties of the shear-thinning fluids are the same as those of the experimental fluids shown in Table 1. The viscosity of the Newtonian fluids is 0.77 Pa·s, and their densities are the same as those of the shear-thinning fluids.

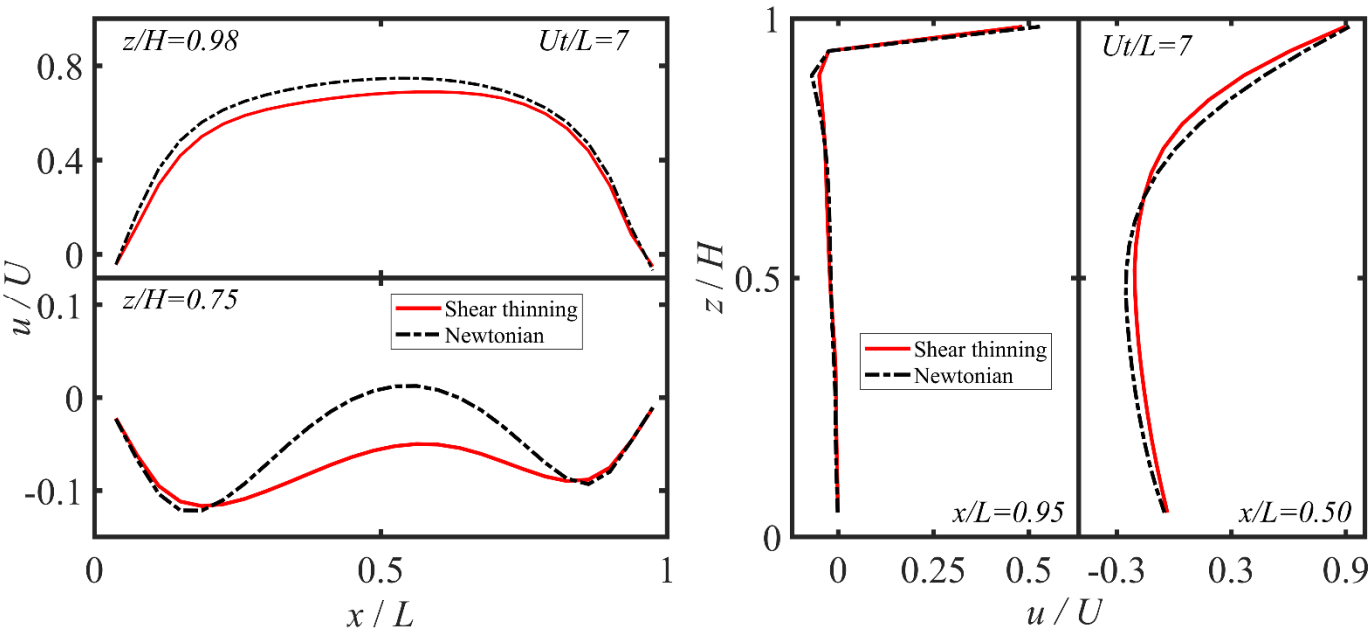

Fig. 8 Simulated instantaneous velocity in x direction u/U at Ut/L = 7 on two horizontal lines (z/H = 0.95 and z/H = 0.75) and two vertical lines (x/L = 0.95 and x/L = 0.50). The cavity was filled with two miscible shear-thinning fluids and Newtonian fluids with the same Reynolds number Re=1.70.

As shown in Fig. 8, the dimensionless x-velocity u/U on two horizontal lines (z/H = 0.75 and z/H = 0.95) and two vertical lines (x/L = 0.50 and x/L = 0.95) at Ut/L = 7 are chosen to present quantitative comparisons results between the Newtonian fluids and shear-thinning fluids. The u/U of the shear-thinning fluids is slightly lower than that of the Newtonian fluids near the lid at z/H = 0.95. At z/H=0.75, the velocity profiles are quite different, which is caused by the different positions of the two circulations, as shown in Fig. 7(b). From the u/U profiles along z/H at x/L = 0.50, we find that the velocity gradient of the shear-thinning fluids near the lid is higher than that of the Newtonian fluids.

Near the lid, the shear rate of the shear-thinning fluid is higher than that of the Newtonian fluid (see Fig. 9(a) and (b)), which is consistent with the above-mentioned distribution of velocity gradient at x/L = 0.50. The apparent viscosity of shear-thinning fluid varies with shear rate, and the higher the shear rate, the lower the apparent viscosity, as shown in Fig. 9(a), (c) and (d). In our previous work on the lid-driven cavity with two miscible Newtonian fluids, we found that better mixing could be obtained by increasing the viscosity of

the fluids [25]. Area averaged apparent viscosity of Fig. 9(d) is 0.49 Pa·s, and it is smaller than the viscosity of the Newtonian fluids 0.77 Pa·s, which might be the reason that the mixing and momentum transport of the shear-thinning fluids are slower than those of the Newtonian fluids at constant *Re* shown in Fig. 7.

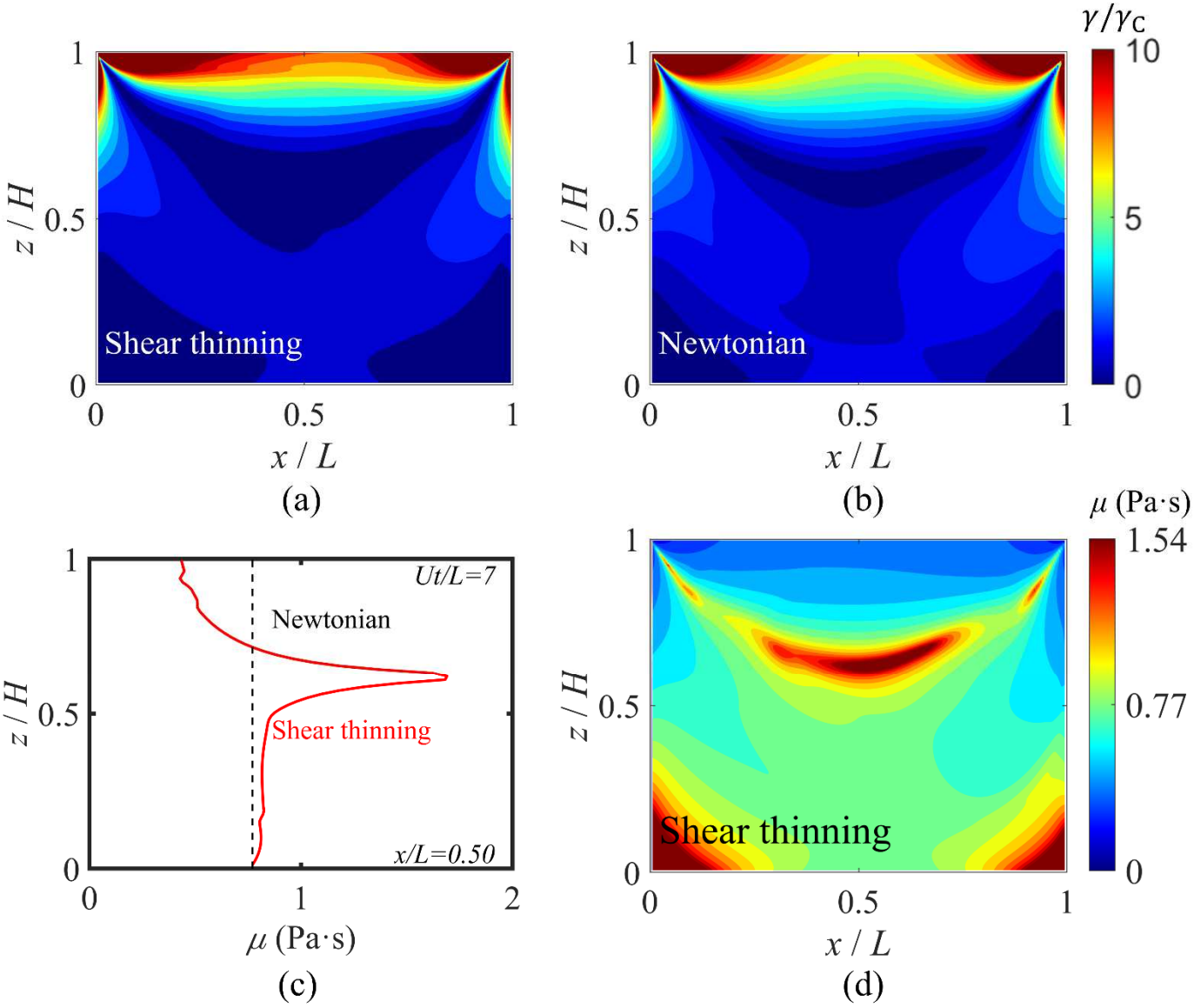

Fig. 9. Simulated instantaneous shear rate field of two miscible shear-thinning fluids (a) and Newtonian fluids (b) at Ut/L = 7 with constant Reynolds number Re=1.70. (c) Viscosity of the Newtonian fluids in black and apparent viscosity of the shear-thinning fluids in red at x/L = 0.50, Ut/L = 7, and Re=1.70. (d) Apparent viscosity distribution of the shear-thinning fluids in the plane y=0 at Ut/L = 7 and Re=1.70.

5.3. Effects of different parameters on mixing

To explore the mechanism of mixing, we will investigate the effect of parameter variation mentioned above on the mixing process in this section. Because of limitations on the lid displacement in our

experiments, the flow only evolves until Ut/L = 7. The mixing process in the simulations was extended to Ut/L = 16.

The mixing efficiency is quantitatively described by the intensity of segregation (IOS) in the mid-plane of the cavity [36]:

$$\mathrm{IOS} = \frac{\iint_A (\bar{C} - C_i)^2 \mathrm{d}A}{(1-\bar{C})\bar{C}} \tag{12}$$

$$\bar{C} = \frac{\iint_A C_i \mathrm{d}A}{A} \tag{13}$$

where $\bar{C}$ is average scalar concentration over a selected plane and A is the area of the plane (m^2). The IOS has a value between 0 and 1. If IOS = 1, the segregation is complete. When IOS = 0, the concentration in the mid-plane of the cavity is uniform.

Firstly, two identical liquids ($\Delta\rho$ = 0) were placed in LDC to show the mixing cases of miscible shear-thinning fluids that have the same *Re* and *n*, with, however, different *U* and *k*. As shown in Fig. 10(a) and (b), the mixing performance of the cases with different *U* and *k* is very close so that we confirm that indeed this system is determined by *Re* and *n* only, and not by *U* and *k* separately. Then, to investigate how mixing depends om *Re* when fixed *n*, a series of cases were simulated. As shown in Fig. 10(c), the effect of *Re* on IOS is weak and changing the value of *Re* have a little effect on mixing. Therefore, it could be concluded that there is not much impact of *Re* on the flow and therefore on mixing when *Re* is low. In Fig. 10(d), the smaller the value of *n*, the larger the value of IOS at the same time. So, we could assert that the stronger the non-Newtonian characteristics of the shear-thinning fluids, the worse the mixing efficiency under the same condition.

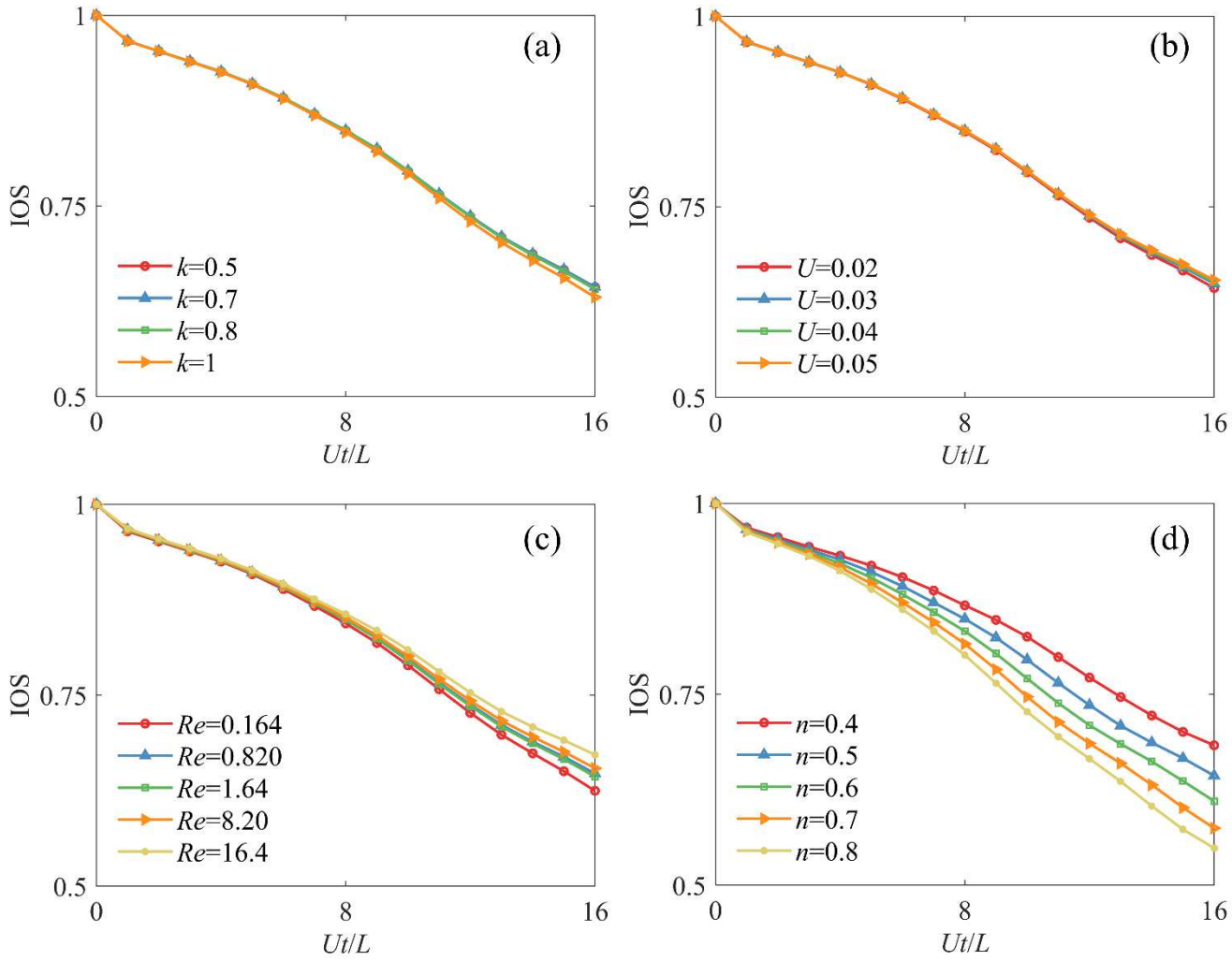

Fig. 10. The instantaneous IOS with different parameters of two identical miscible shear-thinning fluids: (a) n=0.5, U=0.02 m·s^{-1}, Re=1.64, H_1/H=0.25, k=0.5, 0.7, 0.8, 1 Pa·s^n, ρ=1296, 1814, 2073 and 2591 kg·m^{-3}, respectively; (b) k=0.5 Pa·s^n, n=0.5, Re=1.64, H_1/H=0.25, U = 0.02, 0.03, 0.04, 0.05 m·s^{-1}, ρ=1296, 705, 458 and 328 kg·m^{-3}, respectively; (c) k=0.5 Pa·s^n, n=0.5, H_1/H=0.25, Re =0.164, 0.820, 1.64, 8.20, 16.4, ρ=129.6, 648, 1296, 6480 and 12960 kg·m^{-3}, respectively; (d) k=0.5 Pa·s^n, U=0.02 m·s^{-1}, Re=1.64, H_1/H=0.25, n =0.4, 0.5, 0.6, 0.7, 0.8, ρ=1420, 1296, 1183, 1079 and 985 kg·m^{-3}, respectively.

Fig. 11 shows the mixing of two identical miscible shear-thinning fluids at different initial liquid placement. The height of Liquid 1 in the LDC is denoted by H_1, and H_1/H represents the volume fraction of Liquid 1. As the two fluids are identical, the flow fields for different H_1/H are totally the same, as shown in Fig. 11(a). In Fig. 11(b), the smaller the value of H_1/H, the better the mixing efficiency.

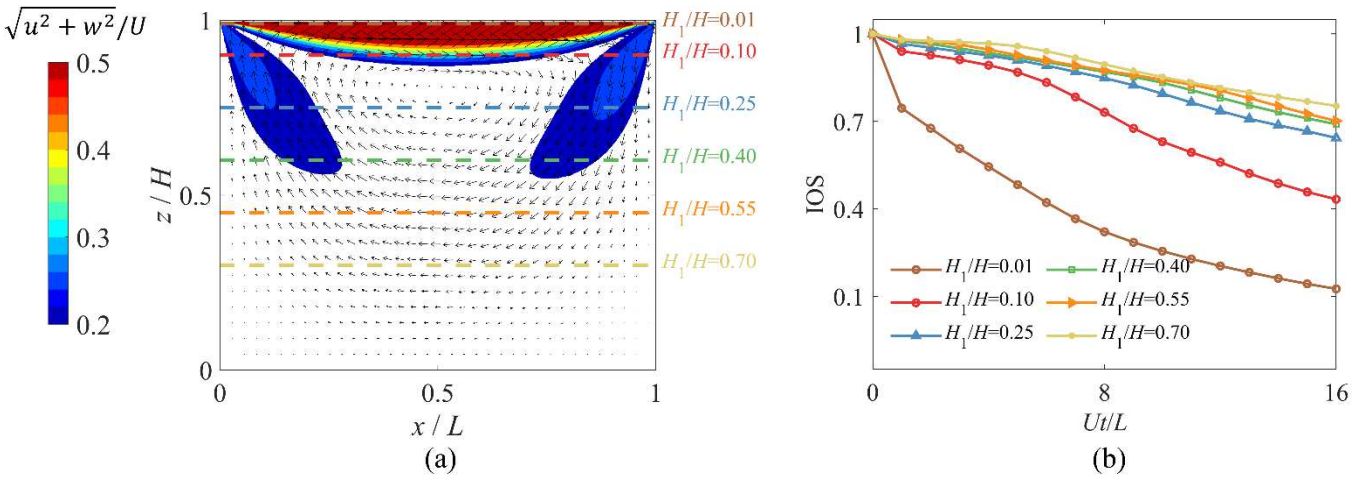

Fig. 11. (a) simulated instantaneous velocity fields in the cavity with different initial liquid placements H_1/H for two miscible shear-thinning fluids with k=0.5 Pa·s^n, n=0.5, ρ=1296 kg·m^{-3}, U=0.02 m·s^{-1}, and Re=1.64. (b) instantaneous IOS for different initial liquid placements H_1/H of two identical miscible shear-thinning fluids.

From now on, we will introduce mixing performance of two shear-thinning fluids with different density ($\Delta\rho\neq0$). As mentioned above, density differences of the two fluids will bring about buoyancy, which cannot be ignored at small Reynolds numbers. In the meantime, it is difficult to evaluate the mixing performance of cases with various density difference and rheological properties. The dimensionless group $\frac{Ar}{Re}=\frac{\Delta\rho g L^{n+1}}{kU^n}$ redefined for shear-thinning fluids in Section 2 could be an alternative for the evaluation.

Fig. 12 shows the time series of IOS for five cases with different power-law indices n. At constant $\frac{Ar}{Re}$, the value of IOS increases with the decrease of n, which means that the mixing performance gets worse. That is, the non-Newtonian characteristics of the shear-thinning fluids slow down the mixing process. Combining the results in Fig. 10(d) at Ar/Re=0 and Fig. 12 at Ar/Re=13.2, we can see that the increasing of buoyance or Ar/Re at constant n will reduce the mixing efficiency. Thus, the mixing of shear-thinning fluids with density difference is quite difficult.

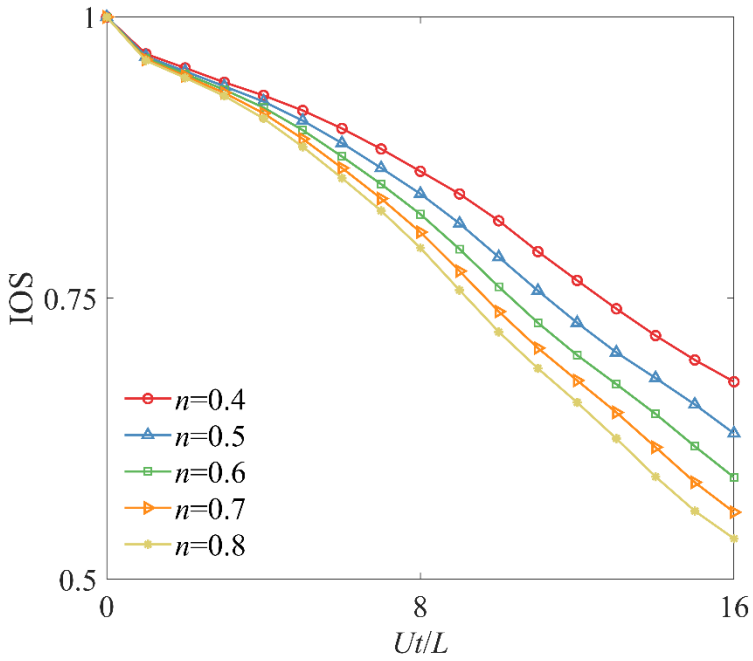

Fig. 12. The instantaneous IOS with different n of two miscible shear-thinning fluids (n =0.4 $\Delta\rho$=9.3 kg·m^{-3}; n = 0.5 $\Delta\rho$=8.5 kg·m^{-3}; n = 0.6 $\Delta\rho$=7.8 kg·m^{-3}; n = 0.7 $\Delta\rho$=7.1 kg·m^{-3}; n = 0.8 $\Delta\rho$=6.5 kg·m^{-3}; H_1/H=0.25, k=0.5 Pa·s^n, U=0.02 m·s^{-1}, Ar/Re=13.2).

Table 2 Parameters of four pairs of cases in Fig. 13

Pair	Ar/Re	Re	k/Pa·s^n	n	$\Delta\rho$/kg·m^{-3}
1	1.32×10^{3}	9.37	0.05	0.8	37
	1.32×10^{3}	4.82	0.1	0.8	74
2	1.32×10^{2}	9.37×10	0.5	0.8	37
	1.32×10^{2}	4.82×10	1	0.8	74
3	1.32×10	9.37×10^{-2}	5	0.8	37
	1.32×10	4.82×10^{-2}	10	0.8	74
4	1.32	9.37×10^{-3}	50	0.8	37
	1.32	4.82×10^{-3}	100	0.8	74

To investigate the effect of $\frac{Ar}{Re}$ on the IOS at constant n, we constructed four pairs of cases by adjusting $\Delta\rho$ and k, as listed in Table 2. The IOS as a function of dimensionless time Ut/L are shown in Fig. 13. At constant $\frac{Ar}{Re}$ and n, the two IOS profiles overlap totally, that is, the dimensionless group $\frac{Ar}{Re}$ could be applied to characterize the mixing process of two miscible shear-thinning fluids with constant power-law index. At constant Ut/L, the higher $\frac{Ar}{Re}$, the larger IOS, which means the mixing of two fluids deteriorates

with increasing $\frac{Ar}{Re}$. In the meanwhile, to achieve the same IOS, it will take more time for the cases with large $\frac{Ar}{Re}$.

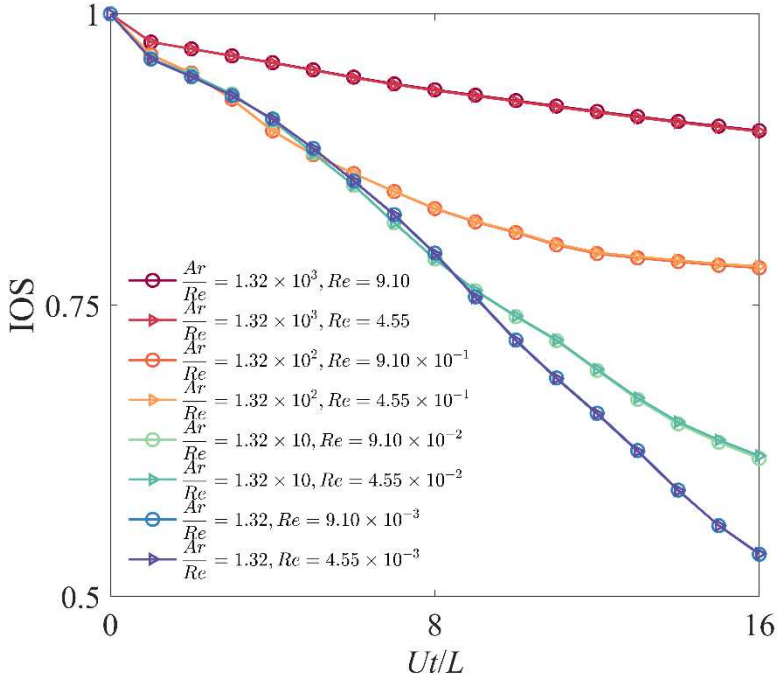

Fig. 13. The instantaneous IOS for cases with different $\frac{Ar}{Re}$. Detailed parameters of four pairs of cases are listed in Table 2.

6. Conclusions

In this work, velocity and concentration fields of two miscible shear-thinning fluids are measured by using PIV and PLIF techniques. Quantitative analyses show that the CFD simulated results of velocity and concentration fields based on the species transport model are in good agreement with the experimental data. Both flow pattern and mixing process for the cases with Newtonian fluid and shear-thinning fluid were compared in detail. At constant Reynolds number and the same moment, the mixing process of the shear-thinning fluids develops slower than that of the Newtonian fluids.

Based on dimensional analyses on mixing in the lid-driven cavity, the dimensionless space of the variation of parameters was analyzed systematically. Then, we used the experimentally validated simulation methods to study the effects of parameters on mixing process in terms of the intensity of segregation as a function of time.

For two identical shear-thinning fluids, the liquid placement condition and the *n* of power-law dominate the process with *Re* playing a marginal role. As for two fluids with density difference, buoyancy will make significant influence on the mixing process. The redefined dimensionless groups $\frac{Ar}{Re}$ was proposed for assessing the effect of buoyancy and rheological properties in mixing of miscible shear-thinning fluids. In a laminar LDC, the mixing performance becomes better with the decrease of $\frac{Ar}{Re}$ and the increase of *n*. In addition, the approximately same mixing process will be obtained at constant $\frac{Ar}{Re}$ and *n*.

Given that the mixing process of shear-thinning fluids exists widely and cavity transfer mixers have extensive application in polymer processing [37,38], future work on the mixing phenomena of shear-thinning fluids in cavity transfer mixers would be of great significance for the design and optimization of polymer blending equipment.

Declaration of Interest Statement

The authors declare that they have no known competing financial interests or personal relationships that could have appeared to influence the work reported in this paper.

Acknowledgements

The financial supports from the National Natural Science Foundation of China (22178014) is gratefully acknowledged.

References

[1] N.P. Cheremisinoff, Mixing practices. Polymer Mixing and Extrusion Technology, Routledge, London, 2017.

[2] G. Beyer, C. Hopmann, Reactive extrusion: Principles and applications, John Wiley & Sons, New York, 2018.

[3] R.S. Hindmarch, The cavity transfer mixer: A blender for all seasonings, Mater. Des. 8 (6) (1987) 331–339.

[4] V.S. Chakravarthy, J.M. Ottino, Mixing of two viscous fluids in a rectangular cavity, Chem. Eng. Sci. 51 (14) (1996) 3613–3622.

[5] P.G.M. Kruijt, O.S. Galaktionov, P.D. Anderson, G.W.M. Peters, H.E.H. Meijer, Analyzing mixing in periodic flows by distribution matrices: Mapping method, AIChE J. 47 (5) (2001) 1005–1015.

[6] H. Mohammadigoushki, S.J. Muller, A flow visualization and superposition rheology study of shear-banding wormlike micelle solutions, Soft Matter 12 (4) (2016) 1051–1061.

[7] T.C. Niederkorn, J.M. Ottino, Chaotic mixing of shear-thinning fluids, AIChE J. 40 (11) (1994) 1782–1793.

[8] M. Alinia, D.D. Ganji, M. Gorji-Bandpy, Numerical study of mixed convection in an inclined two sided lid driven cavity filled with nanofluid using two-phase mixture model, Int. Commun. Heat Mass Transf. 38 (10) (2011) 1428–1435.

[9] Z. Chen, C. Shu, Simplified lattice Boltzmann method for non-Newtonian power-law fluid flows, Int. J. Numer.

Methods Fluids 92 (1) (2020) 38–54.
[10] M. Mamourian, K.M. Shirvan, R. Ellahi, A.B. Rahimi, Optimization of mixed convection heat transfer with entropy generation in a wavy surface square lid-driven cavity by means of Taguchi approach, Int. J. Heat Mass Transf. 102 (2016) 544–554.
[11] A. Syrakos, G.C. Georgiou, A.N. Alexandrou, Solution of the square lid-driven cavity flow of a Bingham plastic using the finite volume method, J. Non Newton. Fluid Mech. 195 (2013) 19–31.
[12] J.M. Buick, Lattice Boltzmann simulation of power-law fluid flow in the mixing section of a single-screw extruder, Chem. Eng. Sci. 64 (1) (2009) 52–58.
[13] F.H. Ling, X. Zhang, Mixing of a generalized Newtonian fluid in a cavity, J. Fluids Eng. 117 (1) (1995) 75–80.
[14] S.S. Mendu, P.K. Das, Flow of power-law fluids in a cavity driven by the motion of two facing lids — A simulation by lattice Boltzmann method, J. Non Newton. Fluid Mech. 175-176 (2012) 10–24.
[15] P. Neofytou, A 3rd order upwind finite volume method for generalised Newtonian fluid flows, Adv. Eng. Softw. 36 (10) (2005) 664–680.
[16] F. Selimefendigil, A.J. Chamkha, Magnetohydrodynamics mixed convection in a lid-driven cavity having a corrugated bottom wall and filled with a non-Newtonian power-law fluid under the influence of an inclined magnetic field, J. Therm. Sci. Eng. Appl. 8 (2) (2016) 021023.
[17] G.R. Kefayati, FDLBM simulation of mixed convection in a lid-driven cavity filled with non-Newtonian nanofluid in the presence of magnetic field, Int. J. Therm. Sci. 95 (2015) 29–46.
[18] G.R. Kefayati, Mesoscopic simulation of magnetic field effect on double-diffusive mixed convection of shear-thinning fluids in a two sided lid-driven cavity, J. Mol. Liq. 198 (2014) 413–429.
[19] R.D. Mills, Numerical solutions of the viscous flow equations for a class of closed flows, J. R. Aeronaut. Soc. 69 (658) (1965) 714–718.
[20] J.R. Koseff, R.L. Street, The lid-driven cavity flow: A synthesis of qualitative and quantitative observations, J. Fluids Eng. 106 (4) (1984) 390–398.
[21] J. R. Koseff, R.L. Street, Visualization studies of a shear driven three-dimensional recirculating flow, J. Fluids Eng. 106 (1984) 21–27.
[22] A. Liberzon, On the effects of dilute polymers on driven cavity turbulent flows, Int. J. Heat Fluid Flow 32 (6) (2011) 1129–1137.
[23] A. Liberzon, Y. Feldman, A.Y. Gelfgat, Experimental observation of the steady-oscillatory transition in a cubic lid-driven cavity, Phys. Fluids 23 (8) (2011) 084106.
[24] H.C.J. Hoefsloot, S.M. Willemsen, P.J. Hamersma, P.D. Iedema, Mixing of two liquids with different rheological behaviour in a lid driven cavity, Proceedings of the 10th European Conference on Mixing, Elsevier, Amsterdam, 2000: 109–116.
[25] F.L. Huang, D.F. Wang, Z.P. Li, Z.M. Gao, J.J. Derksen, Mixing process of two miscible fluids in a lid-driven cavity, Chem. Eng. J. 362 (2019) 229–242.
[26] M. Mansour, Z. Liu, G. Janiga, K.D.P. Nigam, K. Sundmacher, D. Thévenin, K. Zähringer, Numerical study of liquid–liquid mixing in helical pipes, Chem. Eng. Sci. 172 (2017) 250–261.
[27] R. Theunissen, F. Scarano, M.L. Riethmuller, An adaptive sampling and windowing interrogation method in PIV, Meas. Sci. Technol. 18 (1) (2007) 275–287.
[28] I.L. Arbeloa, K.K. Rohatgi-Mukherjee, Solvent effect on photophysics of the molecular forms of rhodamine B. Solvation models and spectroscopic parameters, Chem. Phys. Lett. 128 (5–6) (1986) 474–479.
[29] J.P. Crimaldi, Planar laser induced fluorescence in aqueous flows, Exp. Fluids 44 (6) (2008) 851–863.
[30] S. Haeri, S.H. Hashemabadi, Three dimensional CFD simulation and experimental study of power law fluid spreading on inclined plates, Int. Commun. Heat Mass Transf. 35 (8) (2008) 1041–1047.

[31] R.B. Bird, W.E. Stewart, E.N. Lightfoot, Transport Phenomena, John Wiley & Sons, New York, 2006.

[32] P.C. Murugan, S.J. Sekhar, Species—Transport CFD model for the gasification of rice husk (Oryza Sativa) using downdraft gasifier, Comput. Electron. Agric. 139 (2017) 33–40.

[33] R.R. Irani, A.W. Adamson, Transport processes in binary liquid systems, J. Phys. Chem. 62 (12) (1958) 1517–1521.

[34] M. Hamidipour, J.W. Chen, F. Larachi, CFD study and experimental validation of trickle bed hydrodynamics under gas, liquid and gas/liquid alternating cyclic operations, Chem. Eng. Sci. 89 (2013) 158–170.

[35] J.H. Ferziger, M. Perić, R.L. Street, Computational Methods for Fluid Dynamics, Springer, Cham, 2020.

[36] P.V. Danckwerts, The definition and measurement of some characteristics of mixtures, Appl. Sci. Res. Sect. A 3 (4) (1952) 279–296.

[37] F.L. Huang, P. Chen, J.H. Wang, Z.P. Li, Z.M. Gao, J.J. Derksen, Refractive index-matched PIV experiments and CFD simulations of mixing in a complex dynamic geometry, Ind. Eng. Chem. Res. 59 (16) (2020) 7982–7992.

[38] S.W. Wang, P. Xue, M.Y. Jia, J. Tian, R. Zhang, Effect of polymer blends on the properties of foamed wood-polymer composites, Materials 12 (12) (2019) 1971.